

# Out-of-plane buckling of boundary regions in planar RC structural walls: an approach to prevent instability

Jessica Sarango<sup>1,2</sup>, Ana G. Haro<sup>2,3</sup>, Paúl Acuña<sup>1,2,3</sup>, Pablo Caiza<sup>2,3</sup>

<sup>1</sup> Civil Engineering Career, Universidad de las Fuerzas Armadas ESPE

<sup>2</sup> Department of Earth Sciences and Construction, Universidad de las Fuerzas Armadas ESPE

<sup>3</sup> Structures and Construction Research Group (GIEC), Universidad de las Fuerzas Armadas ESPE

## ABSTRACT

Despite the slenderness that usually characterizes planar RC structural walls, these structural elements effectively resist significant in-plane earthquake demands. However, during the 2010 Chile and 2011 New Zealand earthquakes, some medium to high-rise buildings exhibited out-of-plane buckling instability, a failure mode that had only been observed in experiments. This failure mode was first studied in the 1980s; however, it was just after the recent earthquakes that several studies arose to improve design procedures to avoid future damage. Parameters as the height-to-thickness ratio, reinforcement content, material properties, and the hysteretic behavior of the longitudinal steel have been identified as critical for the onset of buckling instability. In this paper, the influence of the concrete cover was studied through a fiber-based element parametric analysis conducted on 120 RC prisms that simulate boundary elements of special RC walls. The prisms were subjected to incremental axial cyclic loading that mimics the effects of in-plane lateral displacements. As a result, a new approach is presented to limit tensile strains developed in the longitudinal reinforcement of boundary zones to prevent the onset of out-of-plane buckling instability.

**Keywords:** Out-of-plane buckling instability, Boundary elements, Reinforced concrete structural walls, Concrete cover

### Corresponding Author:

Ana Gabriela Haro,  
Department of Earth Sciences and Construction,  
Universidad de las Fuerzas Armadas ESPE,  
Av. General Rumiñahui s/n y Ambato.  
E-mail: agharo@espe.edu.ec

## 1. Introduction

On February 27, 2010, Chile endured an 8.8 Mw earthquake, with a maximum recorded peak ground acceleration (PGA) of 0.65g in the NS direction [1], affecting more than 300,000 structures [2]. In New Zealand, on February 22, 2011, a 6.2 Mw earthquake with a 0.85g PGA in the UP direction [3] damaged more than 100,000 buildings [2]. Some medium to high-rise wall and dual RC buildings exhibited out-of-plane buckling (OPB) instability on their RC structural walls (RCSW) [4-7]. This failure mode concentrates the most significant damage on the end zones of planar walls (see Fig. 1).

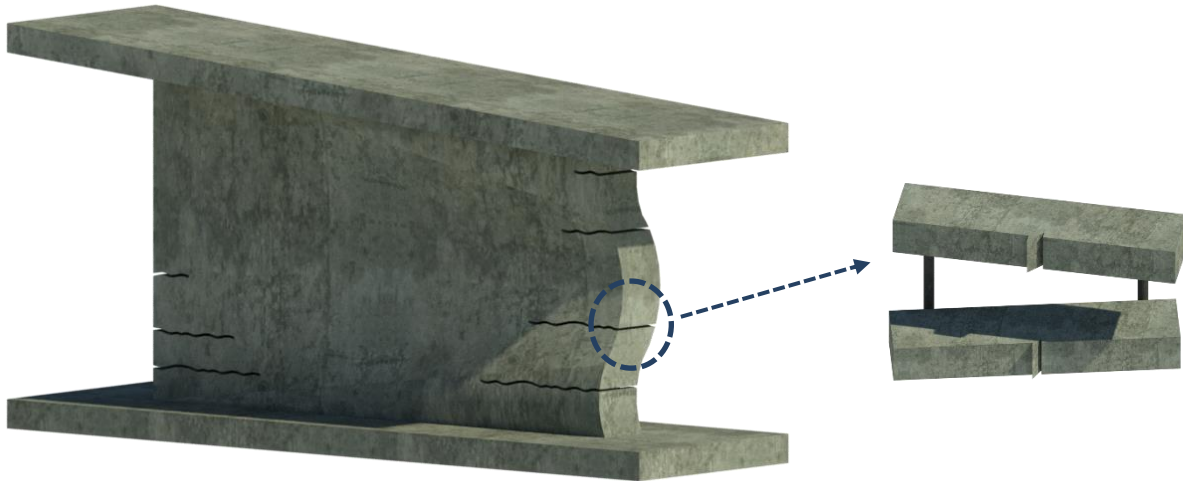


Figure 1. Out-of-plane buckling scheme

The OPB instability of RCSW was studied for the first time by [4]. Here, it was noticed that the longitudinal bars located on the boundary regions served as the only source of stability in the compression zone due to wide cracks that were still open from a previous inelastic tensile demand. This study served as the basis for the phenomenological models proposed by [5] and [6] that associate the effects of in-plane loading with out-of-plane deformations in RCSW to prevent OPB instability.

Based on [6], [7] proposed a less conservative model that limits maximum tensile strains in boundary elements (BE) of special RCSW. This approach also considered the influence of the longitudinal reinforcement ratio, the height-to-thickness ratio of the end regions, the buckling length, the mechanical properties materials, the experimentally adjusted curvature distribution along the buckling length, and the hysteretic behavior of the longitudinal steel.

It is important to note that all the models mentioned above and the described failure mode are primarily deduced from the assumption of a wall with two layers of reinforcement. However, recent studies [8] have evidenced a wide use of walls with only one layer of reinforcement in Latin America, mainly in Colombia. The latter configuration implies more vulnerability since it is associated with a reduced thickness and, even more important, different patterns that trigger the instability.

The two-layer reinforcement configuration is still the most common in countries such as Chile, where the usage of single-layer walls has been forbidden after various reconnaissance teams' observations. Consequently, this research focused on RCSW reinforced with two layers.

Finally, although more models developed over time (including numerical ones), they have not directly addressed the cover thickness influence, which has been identified as a critical parameter related to the onset of OPB instability on RCSW. The approach presented in this paper includes the effect of the mentioned parameter. For this purpose, a fiber-based parametric study was established for 120 column-type specimens that simulate BE of special RCSW. Different height-to-thickness aspect ratios and longitudinal steel ratios were combined with two cover thicknesses. Finally, a modified version of [7] is presented and compared with experimental results on BE.

The main contributions of this work are listed below:

1. A fiber-based model to simulate the effect of in-plane loading on BE of RCSW.
2. A seismic design approach to predict the OPB instability limit state on RCSW

## 2. Description of the model

The model considered 30 mm and 20 mm concrete covers thickness and 28 MPa and 35 MPa concrete compressive strengths. Also, longitudinal steel reinforcement ratios of 1%, 1.5%, 2.0%, 2.5%, and 3% were

analyzed. A total of 120 BE were modeled in SeismoStruct with aspect ratios between  $h/5$  and  $h/30$  that varied with a 5-step increment. First, the design approach by [7] is described.

**2.1. Haro A. G. et al. (2019)**

The model proposed by [7] considers three hysteretic components for the longitudinal reinforcement, see (1), allocated in the extreme regions of RCSW when subjected to in-plane loading. Instability occurs when concrete crushes before cracks close on the opposite side, where the maximum out-of-plane deformations develop once high inelastic levels are reached. In this phase, longitudinal rebar strains are critical parameters that govern out-of-plane instability. Consequently, by estimating  $\epsilon_{sm}$  with the idealized response (see Fig. 2), OPB can be controlled.

$$\epsilon_{sm} = \epsilon_a^* + \epsilon_e + \epsilon_r \tag{1}$$

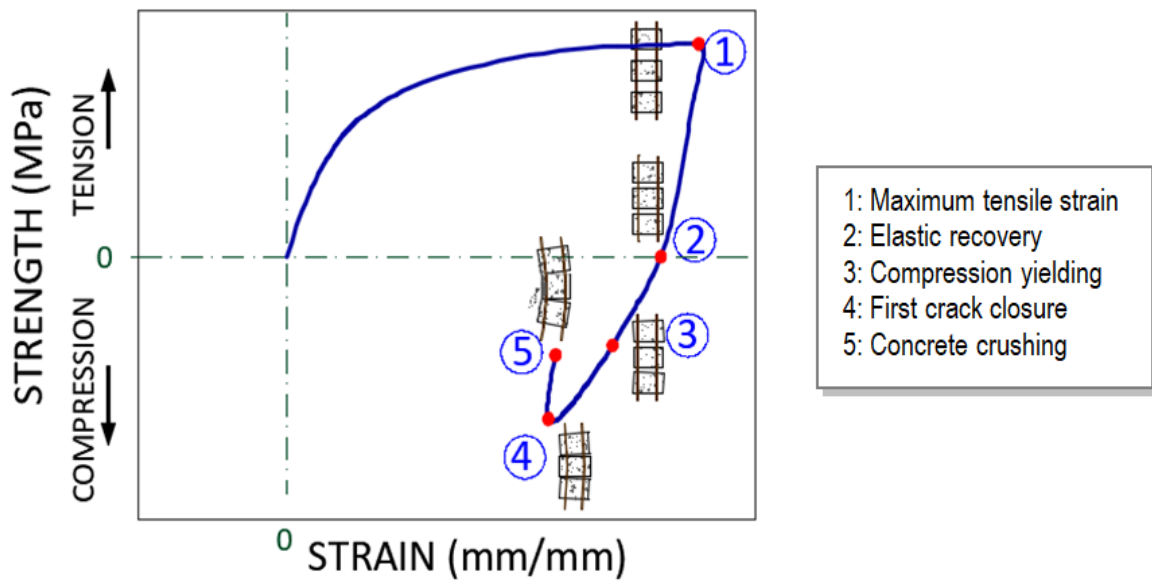


Figure 2. Hysteretic components of longitudinal rebar

In (1),  $\epsilon_a^*$  is the axial strain at first crack closure,  $\epsilon_e$  is the elastic strain recovery that depends on the elastic properties of the concrete and the transfer connection between the steel and concrete, and  $\epsilon_r$  is the reloading strain associated with the compression yielding in both reinforcement layers, which occurs due to the steel stiffness reduction, as a result of the Bauschinger effect [6]. Both  $\epsilon_e$  and  $\epsilon_r$  are expressed as a function of the longitudinal reinforcement yielding strain,  $\epsilon_y$ , as shown in (2), developed by [7].

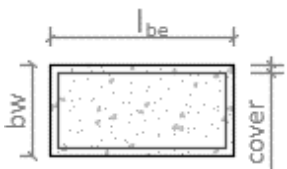
$$\epsilon_{sm} \leq \frac{24}{5} \left(\frac{b_w}{L_o}\right)^2 \cdot \xi_c + \frac{5}{9} \left[ -2.4 + 160 \left(\frac{b_w}{L_o}\right)^2 - 1.9 \ln(\rho_{lbe}) \right] \epsilon_y \tag{2}$$

Where  $b_w$  is the BE thickness,  $L_o$  is the buckling length ( $L_o = h_s / \sqrt{3}$ , being  $h_s$  the clear height),  $\xi_c$  is the stability criterion proposed by [5], which is defined by  $\xi_c = 0.5 \left( 1 + 2.35m - \sqrt{5.53m^2 + 4.7m} \right)$ ,  $m = \rho_{lbe} (f_y / f_c)$  is the mechanical reinforcement ratio,  $\rho_{lbe}$  is the longitudinal steel ratio of the BE, and  $f_y$  and  $f_c$  are the yielding stress of steel and the concrete compression stress, respectively [5].

**2.2. Geometry, detailing, and mechanical properties of materials**

Six geometry types were modeled as presented in Table 1, assuming  $h_s = 3m$  and  $l_{be}$  twice  $b_w$ . According to [7],  $l_{be}$  has no significant impact on the onset of OPB instability when only BE are modeled. The transverse reinforcement,  $A_{st}$ , was calculated according to [10] for special walls that require BE;  $\rho_{lbe}$  took values of 1%, 1.5%, 2%, 2.5%, and 3%.

Table 1. Cross-section details

Geometry	Ratio	$b_w$ (mm)	$l_{be}$ (mm)	Cover (mm)
	h/5	600	1200	20; 30
	h/10	300	600	20; 30
	h/15	200	400	20; 30
	h/20	150	300	20; 30
	h/25	120	240	20; 30
	h/30	100	200	20; 30

The mechanical properties of the materials are shown in Table 2, where  $f_r$  is the fracture stress, and  $E_c$  is the elastic modulus; both calculated as stipulated by [10]. The different geometry types were modeled with two different  $f'_c$ : 28 and 35 MPa.

Table 2. Mechanical properties of materials

Steel		
Parameter	Variable	Value
Yielding stress	$f_y$	420 (MPa)
Elastic Modulus	$E_s$	210000 (MPa)
Yielding strain	$\varepsilon_y$	0.002
Concrete $f'_c = 28$ MPa		
Parameter	Variable	Value
Compression strength	$f'_c$	28 (MPa)
Tensile strength	$f_r$	3.35 (MPa)
Elastic Modulus	$E_c$	25267.13 (MPa)
Concrete $f'_c = 35$ MPa		
Parameter	Variable	Value
Compression strength	$f'_c$	35 (MPa)
Tensile strength	$f_r$	3.74 (MPa)
Elastic Modulus	$E_c$	28249.51 (MPa)

### 2.3. Parametric study

A nonlinear static time-history analysis was conducted in SeismoStruct with a force-based element proved to be a more reliable formulation since it provides an exact solution for prismatic type elements because it is independent of the material constitutive behavior [11], [12]. Six finite elements represented the BE with fixed supports at both ends. Also, the numerical model considered 200 fibers and 6 integration sections.

#### 2.3.1. Loading protocol

The specimens were subjected to axial cyclic loads. Tensile targets were established as a 3-cycle loading depending on  $\varepsilon_y$  fractions until reaching  $\varepsilon_{sm}$ , leading to OPB instability. Compression loads were determined based on the maximum compression capacity of each BE. Fig. 3 shows an example of the loading protocol.

#### 2.3.2. Stress-strain model for steel and concrete

The concrete model used for the simulation was Mander (con\_man) [13], based on [14], for elements confined by stirrups subjected to uniaxial compression. For the reinforcement, the Menegotto & Pinto (stl\_mp) [13] was used, based on [15], which captures the expected cyclic behavior of steel. The adjustment parameters for steel are taken from [9], as shown in Table 3. Here,  $R_o$  controls the transition shape of the curve between the initial

stiffness and post-yielding;  $a_1, a_2$  grade the changes of  $R_o$ ;  $R_n$  is the updated curvature parameter, and  $a_3, a_4$  define how the isotropic hardening is included in the stress-strain material response [13].

### 2.3.3. Failure criteria

As reported by [7], OPB failure occurs when concrete crushing is exhibited in the area where the highest strains develop. Thus, a concrete strain equal to -0.004, as suggested by [9], is used as the failure criterion to stop the analysis.

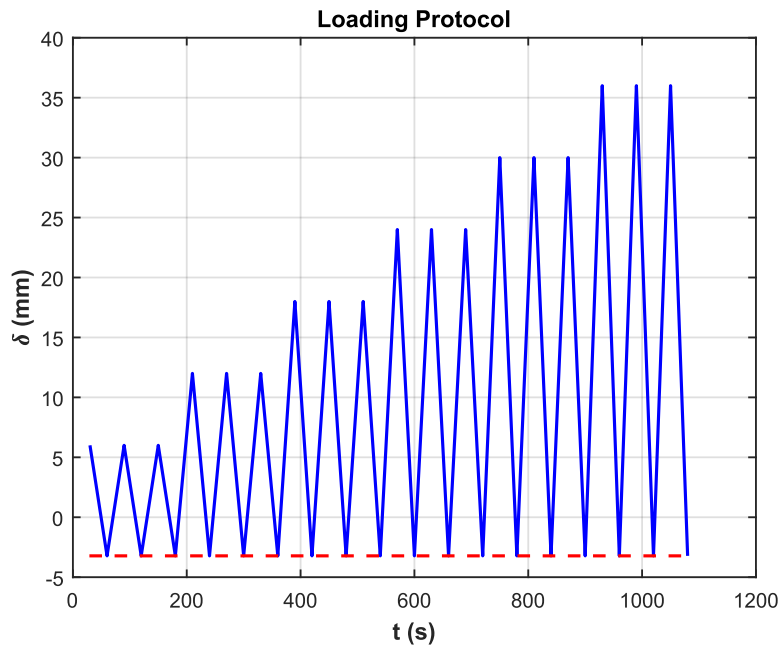


Figure 3. Loading protocol for time history analysis

Table 3. Mechanical parameters of the reinforcement for the modeling in SeismoStruct [9]

Parameter	$a_1$	$a_2$	$a_3$	$a_4$	$R_o$
Value	2.0	18	0.15	0.025	2.0

### 3. Results analysis

The greatest out-of-plane deformations occurred close to  $h_s/2$  since the analysis conducted on this research corresponds to the case of a constant strain gradient. Subsequently, the maximum tensile strains,  $\epsilon_{sm}$ , on each specimen were obtained from the average of these values reached at the center bars (green bars) of the BE as shown in Fig. 4.

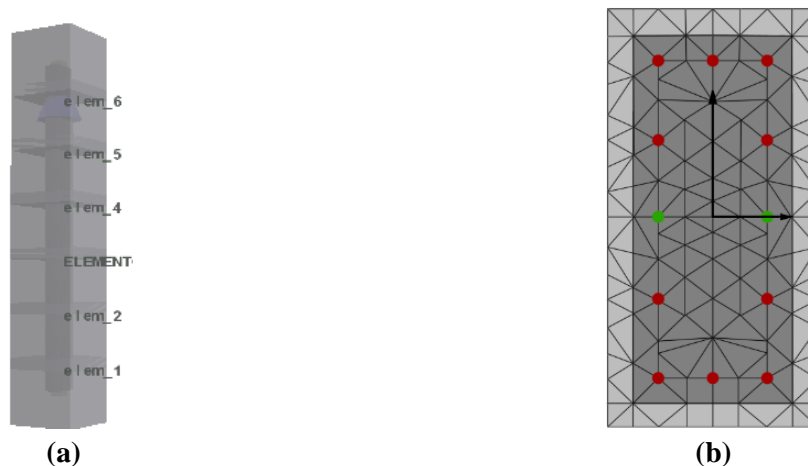


Figure 4. Analysis points for each BE (a) elevation view and (b) plan view [16]

### 3.1. Results

The estimate of  $\varepsilon_{sm}$  was discretized into two parts:  $\varepsilon_a^*$  and  $\varepsilon_e + \varepsilon_r$ , the later expressed as a function of  $\varepsilon_y$  according to [6].

The results from the BE with an aspect ratio of  $h/30$  were discarded due to convergence problems associated with the insufficient cross-section to carry the load cycles before experiencing OPB instability, even though they met the provisions from [10]. Other discarded specimens were those with an  $h/5$  aspect ratio and some with  $h/10$  and  $h_s = 3$  m since that exhibited concrete crushing because of robust cross-sections [16].

### 3.2. Trend functions

Fig. 5 shows the influence of  $\rho_{lbe}$  and  $cov$  on the normalized values of  $\varepsilon_e + \varepsilon_r$  whereas Fig. 6 shows trend functions for  $\% \rho_{lbe}$  vs.  $\varepsilon_{sm}$ , once the results from the BE that presented a different failure mode were removed. Additionally, the predictions for each aspect ratio calculated with Eq. (2), identified as the HKC model, are included. Although the curves presented in Fig. 6 follow a similar polynomial function used by [7], the results suggest an adjustment.

A higher deformation capacity was associated with a smaller concrete cover, attributed to a larger confined area. Also, BE with  $f'_c = 35$  MPa reported increased  $\varepsilon_{sm}$  values and, consequently, improved OPB stability.

As noticed in Fig. 6, the concrete cover is an important parameter that affects the predictions for  $\varepsilon_{sm}$ , so a modification to (2) is suggested. This modification is introduced as the normalized sum of the  $\varepsilon_e + \varepsilon_r$  components. The concrete cover,  $cov$ , is subtracted from  $b_w$  since it decreases the core contribution.

To adjust [7], a linear regression was employed following (3):

$$f(x, y) = p00 + p10 \left( \frac{b_w - cov}{L_o} \right)^2 + \ln(\rho_{lbe}) \tag{3}$$

Equation (3) coefficients that best fit the results from SeismoStruct are obtained from interpolation and extrapolation of the confidence limits. Equation (4) is presented as an adjustment to the normalized sum of the components  $(\varepsilon_e + \varepsilon_r) / \varepsilon_y$ .

$$f(x, y) = -1.40 + 165 \left( \frac{b_w - cov}{L_o} \right)^2 + 1.10 \ln(\rho_{lbe}) \tag{4}$$

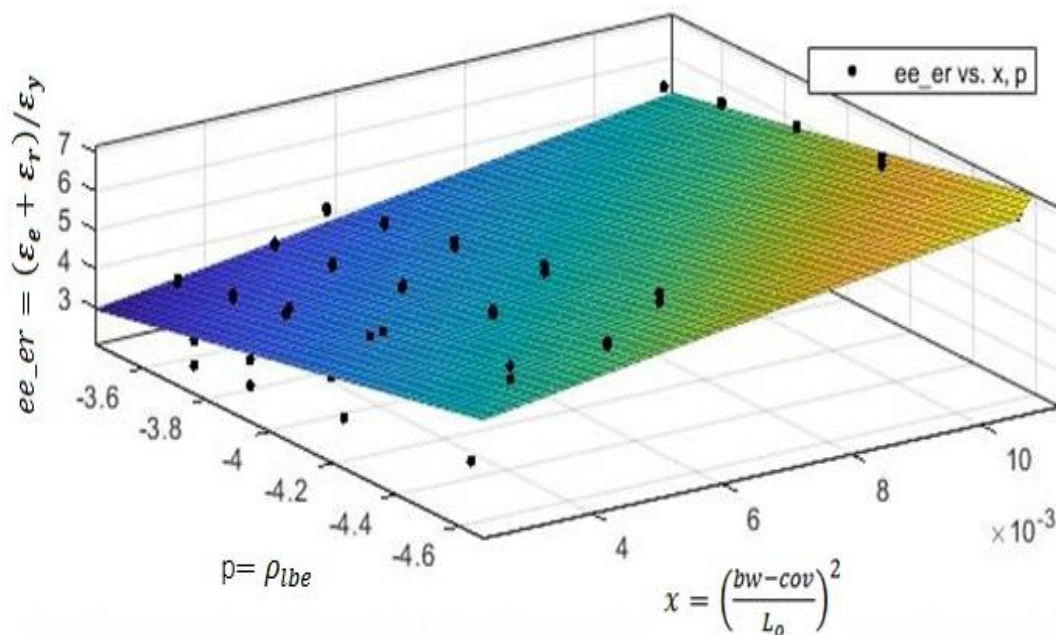


Figure 5. Steel and aspect ratios influence on  $\varepsilon_e + \varepsilon_r$

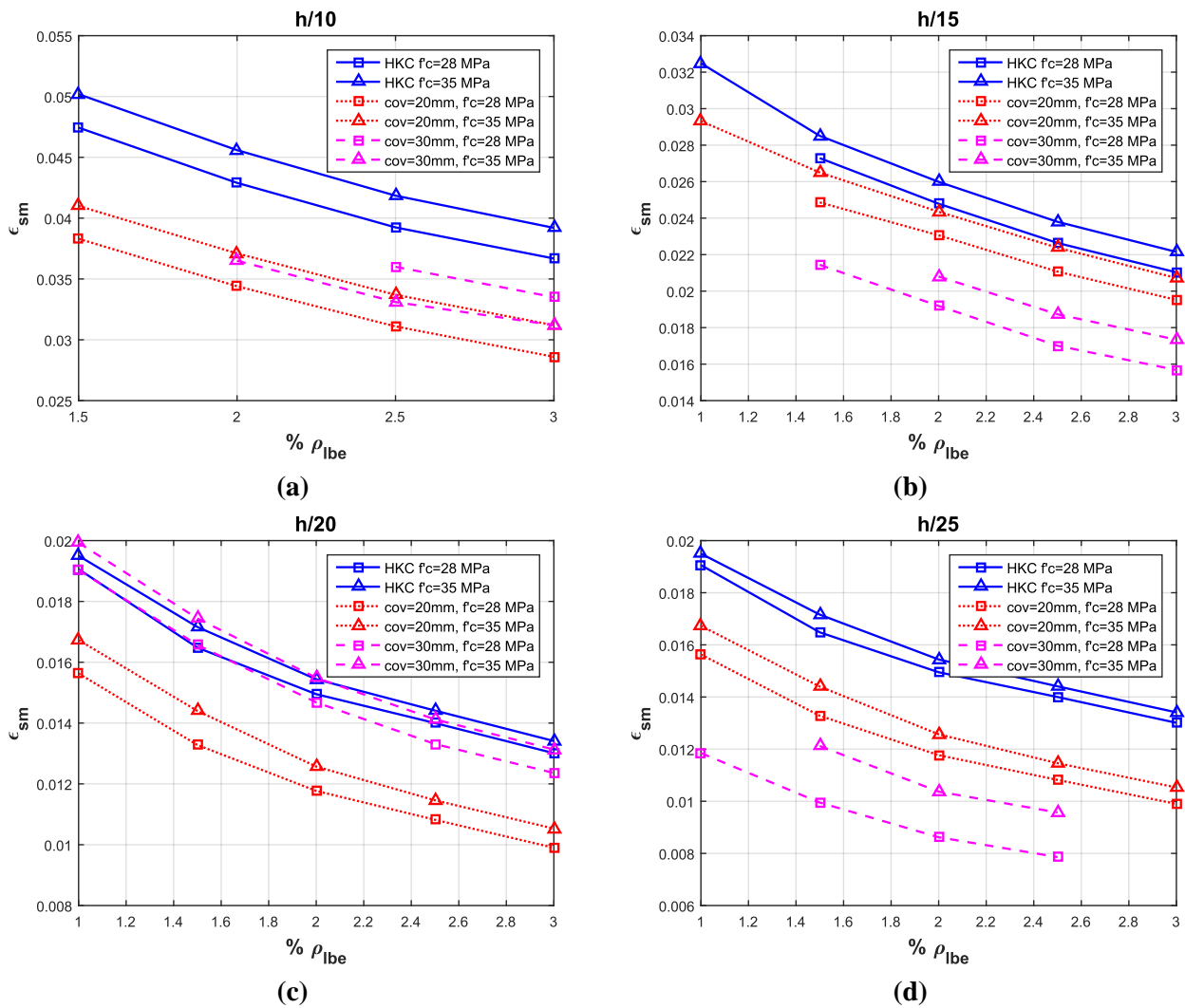
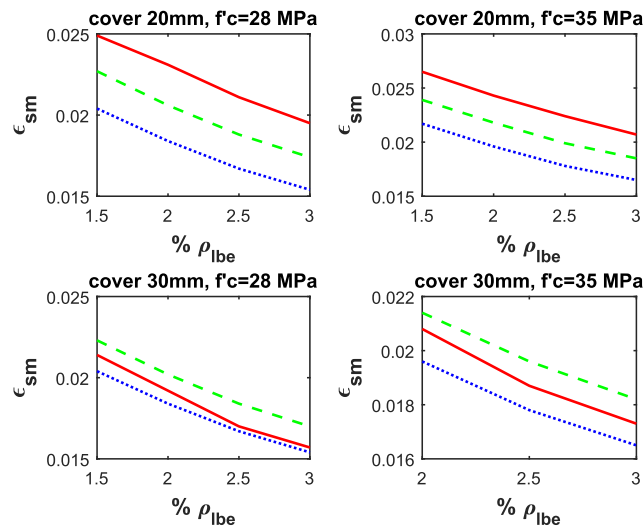


Figure 6. Steel content vs. strain for different aspect ratios

When comparing (2) and (5), there is a difference associated with  $cov$ , which is exhibited on Fig. 7.

$$\epsilon_{sm} \leq \frac{24}{5} \left( \frac{b_w}{L_o} \right)^2 \cdot \xi_c + \left[ -1.40 + 165 \left( \frac{b_w - cov}{L_o} \right)^2 - 1.10 \ln(\rho_{lbe}) \right] \epsilon_y \quad (5)$$





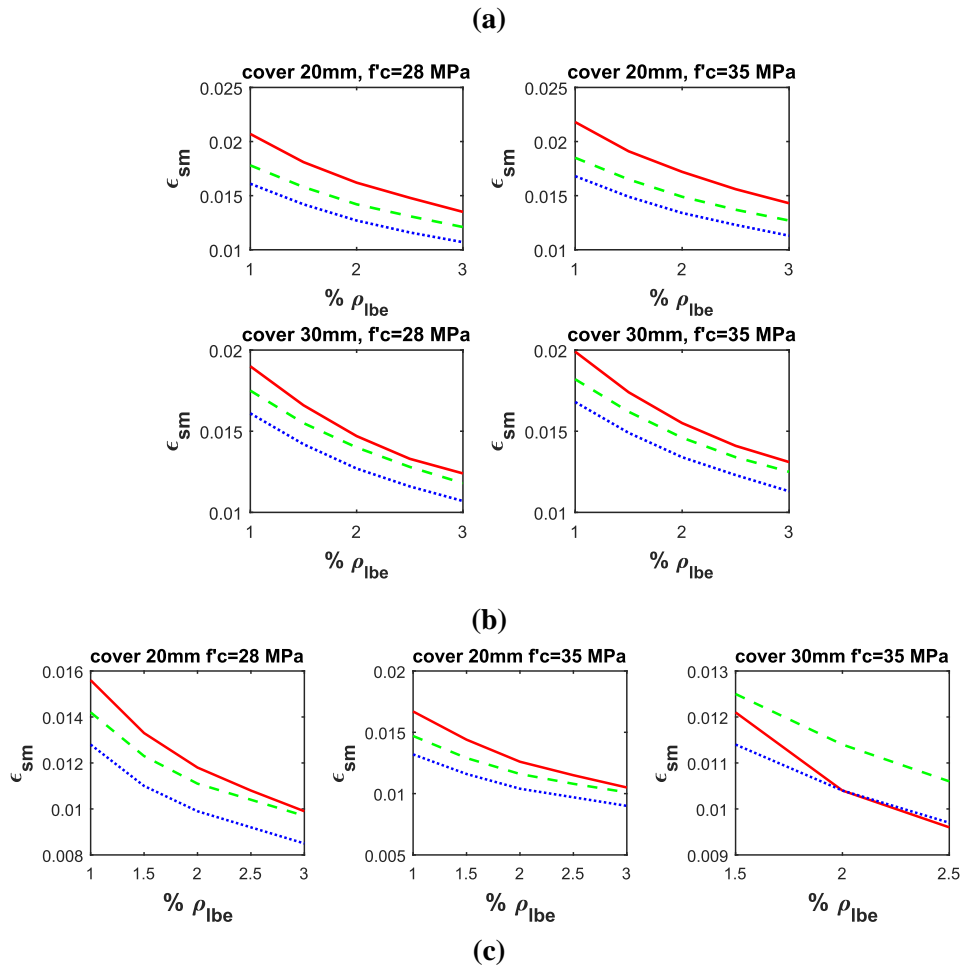


Figure 7. Results: SeismoStruct (solid), (2) by [7] (dot) and (5): new proposal (dash)

(a)  $h/15$ , (b)  $h/20$  y (c)  $h/25$

### 3.3. Proposal validation

A comparison of the results from (5), (2), and the ones obtained in [6] and [9] was developed. The buckling length  $L_o$  was taken as  $h_s$  since the considered boundary conditions were pinned-pinned, contrary to what was considered in [9], see Fig. 8 and Fig. 9. It is observed that the new proposal better approaches the experimental results from [6]. Finally, (2) results more conservative when contrasted with (5) but better approximates the experimental values since [9] excluded the concrete cover.

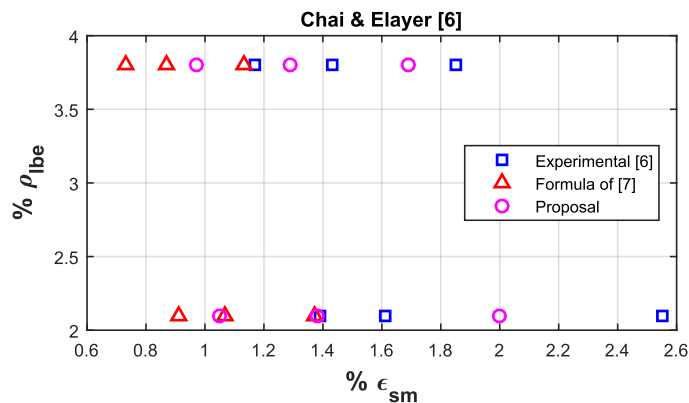


Figure 8. Comparison: Experimental program by [6], (2) by [7], and (5): new proposal



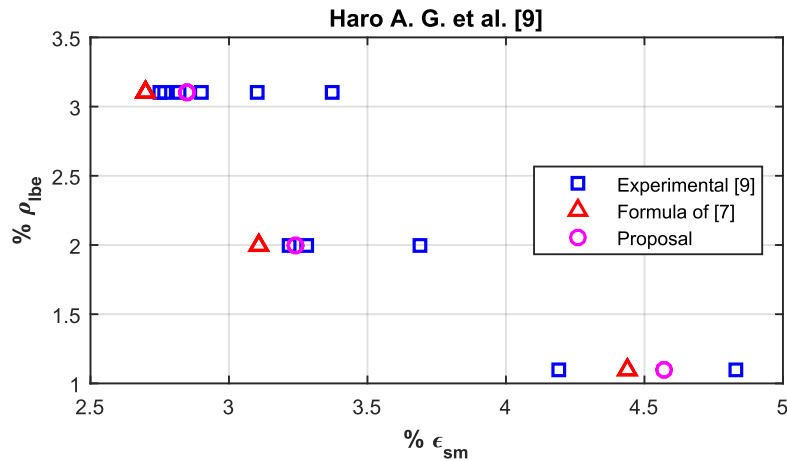


Figure 9. Comparison: Experimental program by [9], (2) by [7], and (5): new proposal

#### 4. Conclusions

This paper has addressed the influence of concrete cover and additional critical parameters on the onset of out-of-plane buckling instability of reinforced concrete structural walls through an analytical study on boundary elements. The main conclusions are described below:

- Concrete cover with higher thickness reduces the capability to exhibit increased tensile strain under cyclic loading, and consequently, out-of-plane instability develops at earlier stages. The same trends were observed for lower concrete cover compression strengths.
- The proposed approach better predicts the onset of buckling instability when compared with the previous model, which does not consider the influence of the concrete cover.
- Boundary elements with the slenderest aspect ratios present out-of-plane buckling instability problems sooner than the thicker ones, corroborating what has been proved through several research programs on the topic.
- Higher longitudinal steel ratios exhibit a reduced out-of-plane buckling stability capacity. When the sections are robust enough and the steel content is minimal, the predominant failure mode is concrete crushing.

#### References

- [1] A. S. Elnashai, B. Gencturk, O. S. Kwon, I. L. Al-Qadi, Y. Hashash, J. R. Roesler, S. J. Kim, S. H. Jeong, J. Dukes, and A. Valdivia, "The Maule (Chile) Earthquake of February 27, 2010: Consequence Assessment and Case Studies," Mid-America Earthquake (MAE) Center, Research Report 10-04, Department of Civil and Environmental Engineering, Univ. Illinois, Urbana-Champaign, Dec. 31, 2010.
- [2] A. Briseño and N. Carreras, "Análisis y diseño de muros estructurales de concreto, considerando las experiencias de los terremotos de Chile 2010 y Nueva Zelanda 2011," Civ. Eng. School, Univ. Católica Andrés Bello, Santiago de Chile, Chile, 2013.
- [3] S. Giovinazzi, W. Thomas, C. Davis, D. Bristow, M. Gallagher, A. Schofield, M. Villemure, J. Eiding, and A. Tang., "Lifelines performance and management following, the 22 February 2010 Christchurch earthquake, New Zealand: Highlights of resilience," *Bulletin of the New Zealand Society for Earthquake Engineering*, vol. 44, no. 4, pp. 402-417, Dec. 2011.
- [4] W. Goodsir, "The design of coupled frame-wall structures for seismic actions," Ph.D. dissertation, Canterbury Univ., Christchurch, New Zealand, 1985.

- [5] T. Paulay and M. J. N. Priestley, "Stability of Ductile Structural Walls," *ACI Structural Journal*, vol. 90, no. 4, pp. 385-392, Jul. 1993.
- [6] Y. H. Chai and D. T. Elayer, "Lateral stability of reinforced concrete columns under axial reversed cyclic tension and compression," *ACI Structural Journal*, vol. 96, no.5, pp. 780-790, Sep. 1999.
- [7] A. G. Haro, M. Kowalsky, and Y. H. Chai, "Out-of-plane buckling instability limit state for boundary regions of special RC structural walls," *Bulletin of Earthquake Engineering*, vol. 17, pp. 5159-5182, Sep. 2019.
- [8] A. Rosso, J. Almeida, and K. Beyer, "Stability of thin reinforced concrete walls under cyclic loads: state-of-the-art and new experimental findings," *Bulletin of Earthquake Engineering*, vol. 14, pp. 455-484, Feb. 2016.
- [9] A. G. Haro, M. Kowalsky, Y. H. Chai, and W. Gregory, "Boundary Elements of Special Reinforced Concrete Walls Tested Under Different Loading Paths," *Earthquake Spectra*, vol. 34, no. 3, pp. 1267-1288, Aug. 2018.
- [10] Building Code Requirements for Structural Concrete and Commentary, ACI 318-14, 2014.
- [11] J. P. Almeida, D. Tarquini, and K. Beyer, "Modelling Approaches for Inelastic Behaviour of RC Walls: Multi-level Assessment and Dependability of Results," *Archives of Computational Methods in Engineering*, vol. 23, pp. 69-100, Mar. 2016.
- [12] M. D'Aniello, F. Portioli y R. Landolfo, "Modelling issues of steel braces under extreme cyclic actions," in *Urban Habitat Constructions under Catastrophic Events*, Naples, 2010, pp. 335-341.
- [13] Seismosoft, SeismoStruct Manual del Usuario, Pavia: Seismosoft Ltda., 2016.
- [14] J. B. Mander, M. J. N. Priestley, and R. Park, "Theoretical Stress-Strain Model for Confined Concrete," *Journal of Structural Engineering*, vol. 114, no. 8, pp. 1804-1826, Sep. 1988.
- [15] M. Menegotto and P. E. Pinto, "Method of Analysis for Cyclically Loaded R. C. Plane Frames Including Changes in Geometry and Non-Elastic Behavior of Elements under Combined Normal Force and Bending," *Symposium on Resistance and Ultimate Deformability of Structures Acted on by Well Defined Repeated Loads*, Zurich, 1973, pp. 15-22.
- [16] J. Sarango, "Efecto del espesor de muros estructurales de hormigón armado con dos capas de reforzamiento en el modo de falla de pandeo fuera del plano," Civ. Eng. School, Univ. de las Fuerzas Armadas - ESPE, Sangolquí, Ecuador, 2019.